Study of the electronic and rovibronic structure of the X 2Σ+, A 2Π, and B 2Σ+ states of AlO

Andrei T. Patrascu, Christian Hill, Jonathan Tennyson, and Sergei N. Yurchenko

Citation: The Journal of Chemical Physics **141**, 144312 (2014); doi: 10.1063/1.4897484
View online: http://dx.doi.org/10.1063/1.4897484
View Table of Contents: http://scitation.aip.org/content/aip/journal/jcp/141/14?ver=pdfcov
Published by the AIP Publishing

Study of the electronic and rovibronic structure of the $X\,^2\Sigma^+$, $A\,^2\Pi$, and $B\,^2\Sigma^+$ states of AlO

Andrei T. Patrascu, Christian Hill, Jonathan Tennyson, and Sergei N. Yurchenko
Department of Physics and Astronomy, University College London, Gower Street, WC1E 6BT London, United Kingdom

(Received 1 June 2014; accepted 29 September 2014; published online 14 October 2014)

The electronic structure of the $X\,^2\Sigma^+$, $A\,^2\Pi$, and $B\,^2\Sigma^+$ states of aluminum monoxide (AlO) are studied via *ab initio* multi-reference configuration interaction calculations. Core correlation corrections, several basis sets, and active space choices are considered. Angular momentum and spin-orbit coupling terms are obtained at different levels of theory. The resulting *ab initio* curves are used to solve the associated rovibronic problem for the total angular momentum J up to 112.5 and then also refined by fitting to the experimental wavenumbers available in the literature, reproducing them with the root-mean-square error of 0.07 cm^{-1}. Theoretical rovibronic energy levels of AlO in its $X\,^2\Sigma^+$, $A\,^2\Pi$, and $B\,^2\Sigma^+$ electronic states are presented including those from the $X - B$ blue-green system.
 [http://dx.doi.org/10.1063/1.4897484]

I. INTRODUCTION

An accurate spectral description of aluminum monoxide (AlO) has become particularly important after the recent discovery of AlO spectral lines in the atmosphere of a new class of the nova-like stars,[1] of which the most prominent examples are probably V838 Mon and V4332 Sgr.[2–4] These two objects defined a new type of eruptive variables called intermediate-luminosity red transients and the observational data showed the intense presence of the $A - X$ system of the AlO radical. Indeed, this $A - X$ band is also found to be fairly prominent in a variety of cool, oxygen rich stars[4] while $B - X$ lines have been observed in sunspots.[5]

AlO emissions are also observed in the Earth's atmosphere, both naturally[6] and as a result of experiments.[7] It is also a major constituent of rocket exhausts; its spectrum is important for monitoring interaction of these gases with the atmosphere.[8,9] It is also used for monitoring reactions involving aluminum and oxygen in the laboratory.[10–13]

In 1927, Pomeroy[14] reported for the first time the resolved rotational structure of the $1 - 0$, $0 - 0$, and $0 - 1$ bands of the blue-green band system of AlO which involved transitions between the $B\,^2\Sigma^+$ and $X\,^2\Sigma^+$ states. In 1937, Sen[15] used higher resolution to reanalyze both the rotational structure of these and a few more bands. He showed that spin-doubling exists in both the upper $B\,^2\Sigma^+$ state and the ground $X\,^2\Sigma^+$ state, and not just in the $X\,^2\Sigma^+$ state as was assumed previously.[14] In 1957, Lagerqvist *et al.*[16] analysed many more bands in the $B - X$ system of AlO and gave precise values for the rotational constants B and D for levels up to $v = 3$ in the B state and up to $v = 5$ in the X state; they also obtained the spin-doubling constants γ for these levels. Mahieu *et al.*[17] excited the blue-green system of AlO in a hollow-cathode discharge cooled by liquid nitrogen. From the difference of the intensity ratios in the $P_2(N)$, $P_1(N)$ and $R_2(N)$, $R_1(N)$ rotational lines with low N, and also from theoretical considerations, they showed that the spin-doubling constant γ in the B state is negative, contrary to the assumptions of the earlier studies.[14,16,17] However, they confirmed that the value of γ in the X state is positive. Later, the rotational structure of ten more bands of the blue-green system, namely, $2 - 0$, $3 - 1$, $4 - 2$, $5 - 3$, $6 - 4$, $7 - 5$, $4 - 1$, $5 - 2$, $6 - 3$, and $7 - 4$ were analysed.[18,19] Singh and Saksena[20] measured line frequencies of unblended intense rotationally resolved lines with an accuracy of 0.05 cm^{-1}. Since that time a series of studies have extended both the range and accuracy of the measured vibronic spectrum.[21–23]

Herzberg and Huber[24] listed seven electronic states of AlO, $X\,^2\Sigma^+$, $A\,^2\Pi$, $B\,^2\Sigma^+$, $C\,^2\Pi$, $D\,^2\Sigma^+$, $E\,^2\Delta$, and $F\,^2\Sigma^+$, as having been identified experimentally. A combined analysis of the $A\,^2\Pi \rightarrow X\,^2\Sigma^+$ and $B\,^2\Sigma^+ \rightarrow X\,^2\Sigma^+$ band systems of AlO based on an experimental emission spectrum is given by Launila and Berg[25] who provide an extensive list of measured transition frequencies.

Several theoretical studies of the electronic states of aluminium monoxide have been performed. *Ab initio* and density functional methods were employed by Orlova and Goddard[26] to describe the thermochemistry of AlO. The $X\,^2\Sigma^+$, $B\,^2\Sigma^+$, $D\,^2\Sigma^+$, and $F\,^2\Sigma^+$ states of AlO were studied via *ab initio* configuration interaction (CI) calculations and associated molecular vibration calculations.[27–29] Very recently, Liu and Shi[30] used multi-reference (MR) CI to obtain spectroscopic constants for several low-lying doublet and quartet states of AlO. *Ab initio* state-averaged complete-active-space self-consistent-field (SA-CASSCF)/Multi-Reference Configuration Interaction (MRCI) calculations were performed by Lengsfield, Liu, and co-workers[27,31] for the blue-green system $B\,^2\Sigma^+ - X\,^2\Sigma^+$. The most recent *ab initio* study of the X and B states, which characterized the potential energy curves (PECs), vibrational energies, spectroscopic constants, dipole moments, using MRCI wavefunctions, was reported by Honjou.[29] We compare our results with the theoretical work of Honjou[29] and that of Zenouda *et al.*[32] in which extended CASSCF (averaging 12 electronic states) and MRCI approaches were used.

Our goal is to generate all components of the Schrödinger equation plus diagonal and off-diagonal effects due to relativity (see below) required for an accurate description of the electronic systems involving the three lowest electronic states $X\,^2\Sigma^+$, $A\,^2\Pi$, and $B\,^2\Sigma^+$ of AlO, including the potential energy curves, spin-orbit curves (SOCs), and electronic angular momentum curves (EAMCs), EAMCs are obtained as matrix elements of the electronic angular momentum operator, $\hat{\mathbf{L}}$, which together with SOCs participate in the couplings between the electronic states. The *ab initio* PECs, SOCs, and EAMCs are then refined by fitting to the experimental data for $^{27}Al^{16}O$ due to Saksena *et al.*,[23] and Launila and Berg[25] with the total angular momentum quantum number J ranging up to 112.5. This is the first step towards providing a comprehensive line list for hot AlO as part of the ExoMol project.[33] This project has already provided line lists for BeH, CaH, MgH,[34] SiO,[35] and NaCl and KCl,[36] but AlO is the first system for which it is necessary to consider strongly coupled PECs.

The paper is structured in the following way. Section II presents the *ab initio* methods, where special attention is given to their effectiveness in the calculation of potential energy curves, the selection of the basis sets and of the active space. The methods used to solve the rovibronic problem are described in Sec. III. The results of the refinement of the *ab initio* potential energy and coupling curves by fitting to the experimental data from the literature are given in Sec. IV.

II. CONFIGURATION INTERACTION CALCULATIONS

Increase in computational power has allowed many improvements of the theoretical results obtained through *ab initio* methods. This is in part also due to the fact that new methods have been implemented and became standard tools in quantum chemistry. In this paper, we use the multi-configuration self-consistent field (MCSCF) method in conjunction with the subsequent MRCI method and the following basis sets: aug-cc-pV(X)Z (X = Q,5,6) for the main calculations and aug-cc-pCVQZ for the core-correlation adapted calculations. These calculations were performed using the MOLPRO electronic structure package[37,38] and the Gaussian basis sets defined therein.

In this paper, we shall follow the MOLPRO notation in order to classify different electronic configurations. In this notation, the total number of closed shell orbitals is separated into orbitals belonging to different representations of the C_{2v} point symmetry group.

The six closed shell orbitals considered here are grouped in the symmetry representations of C_{2v} as follows: four a_1 orbtials, one b_1 orbital, one b_2 orbital, and no a_2 orbitals. The five further orbitals that constituted the active space had symmetries: three a_1 orbitals, one each of b_1,b_2 and no a_2 orbitals. This orbital set is called (7,2,2,0) or (7,2,2).

Molecular properties determined here are presented in Tables I and II where they are compared to those from the theoretical studies of Honjou,[28,29] Zenouda *et al.*,[32] and the experimental work of Launila and Berg.[25] Although the accuracy of the predictions obtained is comparable to that of previous theoretical work, such as that of Honjou,[28,29] it is still far from the experimental accuracy.

TABLE I. Bond lengths, R_e (Å), for the first three electronic states of AlO computed.

State	*Ab in.*[a]	*Ab in.*[b]	Refined[a]	Expt.[c]
$X\,^2\Sigma^+$	1.6341	1.623	1.6189	1.6179
$A\,^2\Pi$	1.7831	1.777	1.7691	1.7678
$B\,^2\Sigma^+$	1.6838	1.677	1.6681	1.6670

[a]This work.
[b]Reference 32.
[c]References 24 and 39.

We have also tested the configurations in the form (8,3,3) and (9,4,4) and the augmented correlation consistent polarized valence-only basis sets up to 6Z. Inclusion of relativistic and core corrections leads to an overall and significant decrease in the energy of the system, but this mostly amounts to a global shift of the potential energy curves and gives corrections that are small with respect to the experimental error. In particular, Table II gives results obtained using a variety of different high-level *ab initio* models. None of the results even begin to approach spectroscopic accuracy. There is an additional problem in that the more demanding models gave off-diagonal terms, relativistic couplings, or transitions dipole moments, which were far from smooth. It is not really possible to work with such curves. For this reason, the results of Table II were all obtained using our final, refined couplings given below. We found that the improvements on the potential energy curve with 5Z and 6Z basis sets do not justify the increased computing time. The same is true for the increased active spaces we tested.

The final choice of the active space was (7,2,2) and an aug-cc-pV4Z which was optimal in terms of performance and smoothness. The computed PECs, SOCs, and EAMCs are presented in Figs. 1 and 3.

As already mentioned, smoothness of the curves is far from guaranteed in these calculations.[41] Here, they are the result of a careful choice of the starting point. We started generating the potential energy functions and implicitly all other geometry dependent properties at the shortest internuclear distance. We continued by successively increasing the bond length R while keeping as an initial configuration the one generated at the previous position. We varied the bond length in the range R = 1.2–2.74 Å.

The off-diagonal *ab initio* couplings and transition dipoles as obtained by MOLPRO are often affected by the ambiguity of phases associated with electronic wavefunctions, which have an arbitrary overall sign for any given geometry. This problem is illustrated in Fig. 2, where raw MOLPRO data for different couplings are shown; a transition dipole moment is also shown for comparison. This ambiguity must be eliminated by a consistent choice of the phases for all the matrix elements. To this end, we chose the phase at the reference geometry of R = 1.84 Å and corrected all MOLPRO matrix elements to be smooth for all geometries, see Fig. 2. The corrected *ab initio* SOCs and EAMCs are also shown in Fig. 3.

TABLE II. $J = 0$ energy term values and electronic excitation energies obtained using different high-level *ab initio* treatments compared to the refined values (this work) observed values.[39,40] All data in cm^{-1}. All calculations at MRCI level.[a]

State	Vib	pVQZ (8,3,3)[b]	pVQZ(8,3,3)MVD[c]	pV5Z(8,3,3)DK[d]	pVQZ(9,4,4)[e]	Obs.	Refined
$X^2\Sigma$	1	949.98	948.70	957.04	944.56	965.45	965.44
$X^2\Sigma$	2	1887.62	1884.98	1899.06	1874.18	1916.86	1916.85
$X^2\Sigma$[b]	3	2808.61	2804.54	2825.96	2788.94	2854.24	2854.21
$X^2\Sigma$	4	3711.43	3706.17	3737.70	3689.03	3777.50	3777.50
$X^2\Sigma$	5	4599.10	4593.61	4634.29	4574.71	4686.71	4686.66
$X^2\Sigma$	6	5464.35	5469.44	5515.82	4684.94	5581.93	5581.91
$X^2\Sigma$	7	6346.30	6332.07	6382.48	5396.53	6463.13	6463.04
$A^2\Pi$	1	724.42	711.58	…	…	720.94	720.82
$A^2\Pi$	2	1410.20	1414.35	…	…		1432.88
$A^2\Pi$	3	2106.85	2108.41	…	…		2137.03
$A^2\Pi$	4	2793.83	2793.84	…	…		2813.05
$A^2\Pi$	5	3472.25	3470.75	…	…	3512.73	3511.15
$A^2\Pi$	6	4143.50	4139.24	…	…		4189.08
$A^2\Pi$	7	4799.53	4799.44	…	…		4857.90
$B^2\Sigma$	1	847.02	847.03	…	…	863.11	862.99
$B^2\Sigma$	2	1688.34	1688.35	…	…	1718.85	1718.87
$B^2\Sigma$	3	2525.03	2525.04	…	…	2567.28	2567.36
$B^2\Sigma$	4	3355.99	3356.01	…	…	3408.41	3408.44
$B^2\Sigma$	5	4178.57	4178.59	…	…	4242.18	4242.14
$B^2\Sigma$	6	4990.40	4990.42	…	…	5068.65	5068.52
$B^2\Sigma$	7	5791.98	5792.00	…	…	5887.79	5887.64
T_e(X-A)	…	4839.99	4803.18	…	…	5406.00	5406.00
T_e(A-B)	…	15 387.67	15 424.48	…	…	15 283.00	15 282.00

[a]For the 5-zeta and increased (9,4,4) active space models, only the ground state has been calculated.
[b]Main model: MRCI calculation with aug-cc-pVQZ basis set (8,3,3) active space.
[c]Main model plus MVD1 relativistic correction.
[d]Main model plus 5-Z basis set and Douglas-Kroll relativistic correction.
[e]Main model plus increased (9,4,4) active space.

The *ab initio* EAMCs and SOCs between the electronic states are particularly important in the region around the crossings between the states in question. The angular momentum matrix elements have been calculated from the wavefunctions obtained after the MRCI cycle. The level of theory used is the same as for the potential energies. The spin-orbit (SO) matrix elements were calculated using the full Breit-Pauli operator as implemented in the MOLPRO package. The results of the spin-orbit and EAM calculations are illustrated in Table III, where some equilibrium SO values are compared to the values from the literature.[39,42,43] The agreement is reasonable in all cases. A factor $\sqrt{2}$ must be applied to the value of $H_{el}^{SO}(X - A)$ from Launila and Jonsson[39] in order to agree with our definition of the off-diagonal SO constant $\langle X\,^2\Sigma^+|\hat{H}_{SO}|A\,^2\Pi\rangle$. As a reference, the atomic limit of the spin-orbit coupling is 56.3 cm^{-1} which is half energy splitting of ground state atomic aluminum 112.061 cm^{-1}.[43]

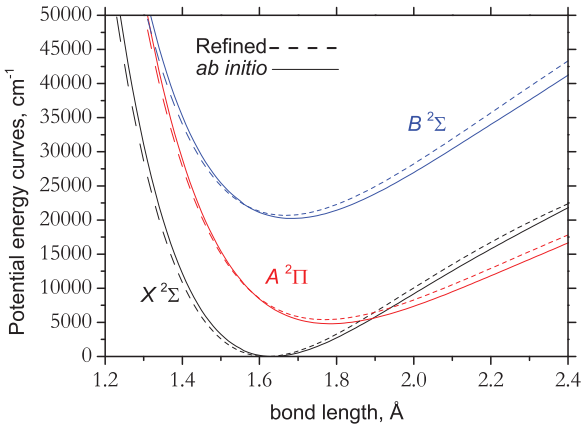

FIG. 1. *Ab initio* and refined potential energy curves (cm^{-1}) for the first three electronic states of AlO.

III. ROVIBRONIC PROBLEM

Although solution of the uncoupled diatomic nuclear motion problem is standard,[44] there appears to be no general program available for solving the coupled problem. We have therefore developed a new program, DUO, to address this problem. DUO is a flexible, multistate program full details of which will be reported elsewhere.[45] Here, we concentrate on aspects of the program important for AlO.

Within the Born-Oppenheimer approximation, the SO free Hamiltonian of the diatomic problem in the absence of the hyperfine splitting is[46]

$$\hat{H}_{tot} = \hat{H}_e + \hat{H}_r + \hat{H}_v, \quad (1)$$

where $\hat{H}_e$ is the electronic part, $\hat{H}_r$ is the rotational part, and $\hat{H}_v$ is the vibrational part. The rotational angular momentum $\hat{\mathbf{R}}$ is perpendicular to the internuclear axis. Considering Hund's case (a) and representing the rotational

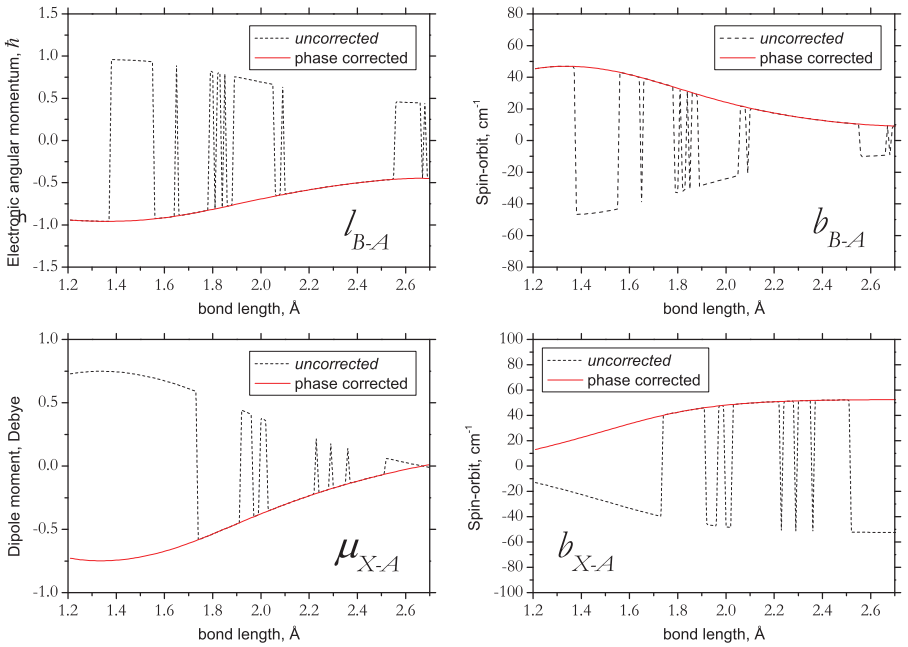

FIG. 2. Phase correction for the off-diagonal couplings and transition dipoles. See text for the definition of l_{B-A}, b_{X-A}, b_{B-A}, and μ_{X-A}.

angular momentum as

$$\hat{\mathbf{R}} = \hat{\mathbf{J}} - \hat{\mathbf{L}} - \hat{\mathbf{S}} \tag{2}$$

in terms of the total $\hat{\mathbf{J}}$, electronic $\hat{\mathbf{L}}$, and spin $\hat{\mathbf{S}}$ angular momenta and choosing the body-fixed z axis along the internuclear axis the rotational part is given by

$$\begin{aligned}\hat{H}_{\mathrm{r}} = \frac{\hbar^2}{2\mu R^2}\big[&\left(\hat{J}^2 - \hat{J}_z^2\right) + \left(\hat{L}^2 - \hat{L}_z^2\right) + \left(\hat{S}^2 - \hat{S}_z^2\right) \\ &+ \left(\hat{J}_+\hat{S}_- + \hat{J}_-\hat{S}_+\right) - \left(\hat{J}_+\hat{L}_- + \hat{J}_-\hat{L}_+\right) \\ &+ \left(\hat{S}_+\hat{L}_- + \hat{S}_+\hat{L}_+\right)\big],\end{aligned} \tag{3}$$

where $\hat{J}_\pm = \hat{J}_x \pm i\hat{J}_y$, $\hat{S}_\pm = \hat{S}_x \pm i\hat{S}_y$, and $\hat{L}_\pm = L_x \pm iL_y$ are the corresponding angular momentum ladder operators and $\mu = m_A m_B/(m_A + m_B)$ is the reduced mass. The DUO basis set functions are chosen as the product

$$|\text{state}, \Lambda, S, \Sigma, v\rangle = |\text{state}, \Lambda, S, \Sigma\rangle|J, \Omega, M\rangle|\text{state}, v\rangle, \tag{4}$$

where $|\text{state}, \Lambda, S, \Sigma\rangle$ is the electronic function, $|J, \Omega, M\rangle$ is the rotational function, $|\text{state}, v\rangle$ is the vibrational function; "state" is the label identifying the electronic state; Λ, Σ, and Ω are the z axis projections of the electronic, spin, and total angular momenta, respectively, and $\Omega = \Lambda + \Sigma$; M is the

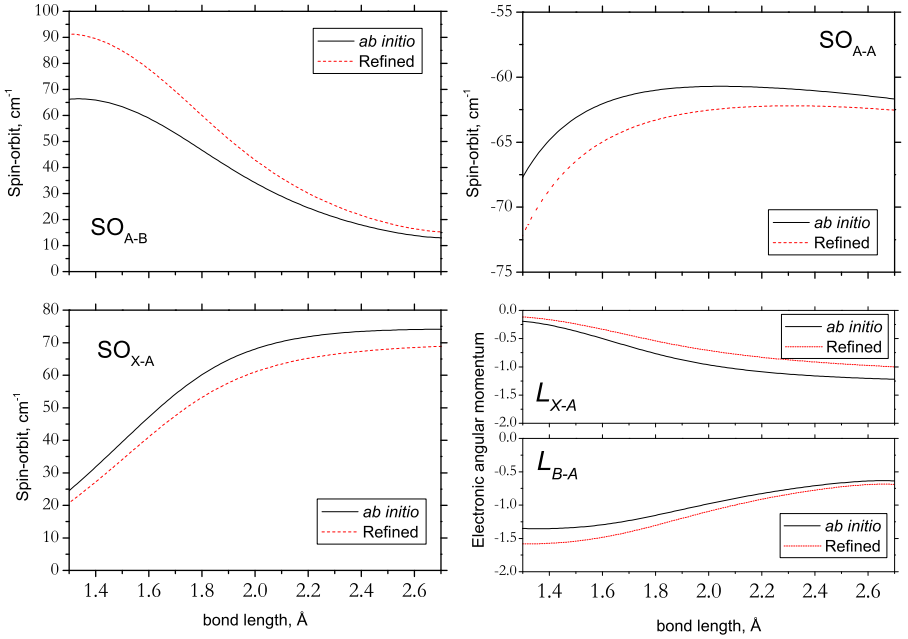

FIG. 3. *Ab initio* and refined SOCs and EAMCs for the three lowest electronic states of AlO.

TABLE III. *Ab initio* and empirical values of SO and EAM matrix elements of $^{27}Al^{16}O$ in cm^{-1} at $R = 1.77$ Å.

	ab initio	Refined	Expt.	Atomic[a]
SO_{A-A} (cm^{-1})	− 61.10	− 63.50	− 63.38[b]	− 56.03
SO_{X-A} (cm^{-1})	41.35	51.60	− 45.66[c]	
SO_{B-A} (cm^{-1})	48.63	62.78		
L_{X-A} (atomic units)	− 0.73	− 0.51	− 0.54[d]	
L_{B-A} (atomic units)	− 1.17	− 1.33		

[a]Obtained as minus half the atomic limit SO-splitting.[43]
[b]The SO constant is related to the experimentally derived value A_e of the ground-vibrational SO-splitting by Launila and Jonsson[39] as $-A_e/2$; our conventions Eqs. (16) and (17) lead a sign change.
[c]Result scaled by $\sqrt{2}$ with respect to Ref. 42.
[d]A sign change due to our conventions Eqs. (13) and (14) is applied to the results of Ref. 42.

projection of the total angular momentum along the laboratory axis Z; v is the vibrational quantum number.

For the rotational basis set, the rigid rotor functions are used, with the following matrix elements:

$$\langle J, \Omega|\hat{J}^2|J, \Omega\rangle = J(J+1), \tag{5}$$

$$\langle J, \Omega|\hat{J}_z|J, \Omega\rangle = \Omega, \tag{6}$$

$$\langle J, \Omega \mp 1|\hat{J}_\pm|J, \Omega\rangle = \sqrt{J(J+1) - \Omega(\Omega \mp 1)}, \tag{7}$$

where M is omitted for simplicity.

The electronic basis functions appear in the solution only implicitly as matrix elements of different components of the operator H_r as well as of the spin-orbit contributions. We choose these basis functions to satisfy the following conditions:[46]

$$\langle \text{state}, \Lambda, S, \Sigma|\hat{L}_z|\text{state}, \Lambda, S, \Sigma\rangle = \Lambda, \tag{8}$$

$$\sigma_v(xz)|\text{state}, \Lambda, S, \Sigma\rangle = (-1)^{s-\Lambda+S-\Sigma}|\text{state}, -\Lambda, S, -\Sigma\rangle, \tag{9}$$

where $\sigma_v(xz)$ is a reflection through the molecular-fixed xz-plane (parity operator) and $s = 1$ for $|\Sigma^-\rangle$ states and $s = 0$ for all other states. The following non-vanishing matrix elements of the spin operators are valid:

$$\langle \Lambda, S, \Sigma|\hat{S}^2|\Lambda, S, \Sigma\rangle = S(S+1), \tag{10}$$

$$\langle \Lambda, S, \Sigma|\hat{S}_z|\Lambda, S, \Sigma\rangle = \Sigma, \tag{11}$$

$$\langle \Lambda, S, \Sigma \pm 1|\hat{S}_\pm|S, \Sigma\rangle = \sqrt{S(S+1) - \Sigma(\Sigma \pm 1)}, \tag{12}$$

where the label "states" is omitted for simplicity.

The non-vanishing and symmetrically unique matrix elements of the ladder angular momentum operator $\hat{L}_+$ as well as of the SO-matrix elements on these basis functions for the three lowest states of AlO $X\,^2\Sigma^+$, $A\,^2\Pi$, and $B\,^2\Sigma^+$ are obtained using MOLPRO and can be summarized as follows:

$$L_{X-A} = \langle X^2\Sigma^+, \Lambda = 0|\hat{L}_+|A\,^2\Pi, \Lambda = -1\rangle, \tag{13}$$

$$L_{B-A} = \langle B\,^2\Sigma^+, \Lambda = 0|\hat{L}_+|A\,^2\Pi, \Lambda = -1\rangle, \tag{14}$$

$$\begin{aligned} SO_{A-A} = \big\langle A\,^2\Pi, \Lambda = 1, \Sigma = \tfrac{1}{2}\big|\hat{H}_{SO}\big|A\,^2\Pi, \\ \Lambda = 1, \Sigma = \tfrac{1}{2}\big\rangle, \end{aligned} \tag{15}$$

$$\begin{aligned} SO_{X-A} = \big\langle X\,^2\Sigma^+, \Lambda = 0, \Sigma = -\tfrac{1}{2}\big|\hat{H}_{SO}\big|A\,^2\Pi, \\ \Lambda = -1, \Sigma = \tfrac{1}{2}\big\rangle, \end{aligned} \tag{16}$$

$$\begin{aligned} SO_{B-A} = \big\langle X\,^2\Sigma^+, \Lambda = 0, \Sigma = -\tfrac{1}{2}\big|\hat{H}_{SO}\big|A\,^2\Pi, \\ \Lambda = -1, \Sigma = \tfrac{1}{2}\big\rangle, \end{aligned} \tag{17}$$

where $S = \frac{1}{2}$ is omitted for simplicity. All other non-vanishing matrix elements can be obtained from Eqs. (13) to (17) by applying the symmetric properties upon the reflection as defined by Eq. (9) and the Wigner-Eckart theorem.

In DUO, the electric dipole moment components μ_α ($\alpha = x, y, z$) should be transformed into the standard irreducible representation as given by

$$\begin{aligned} \mu_0 &= \mu_z, \\ \mu_\pm &= \mp\frac{1}{\sqrt{2}}\left(\mu_x \pm i\mu_x\right). \end{aligned} \tag{18}$$

In this representation, the diagonal and non-diagonal matrix elements of the (transition) dipole moments are

$$\mu_{X-X} = \langle X\,^2\Sigma^+, \Lambda = 0|\mu_0^{X-X}|X\,^2\Sigma^+, \Lambda = 0\rangle, \tag{19}$$

$$\mu_{A-A} = \langle A\,^2\Pi, \Lambda = 1|\mu_0^{A-A}|A\,^2\Pi, \Lambda = 1\rangle, \tag{20}$$

$$\mu_{B-B} = \langle B\,^2\Sigma^+, \Lambda = 0|\mu_0^{B-B}|B\,^2\Sigma^+, \Lambda = 0\rangle, \tag{21}$$

$$\mu_{X-A} = \langle X\,^2\Sigma^+, \Lambda = 0|\mu_+^{X-A}|A\,^2\Pi, \Lambda = -1\rangle, \tag{22}$$

$$\mu_{B-A} = \langle B\,^2\Sigma^+, \Lambda = 0|\mu_+^{B-A}|A\,^2\Pi, \Lambda = -1\rangle, \tag{23}$$

where Σ values ($\Sigma' = \Sigma''$) are omitted for simplicity.

It should be noted that for $\Lambda \neq 0$ the MOLPRO functions are not eigenfunctions of $\hat{L}_z$ as required by Eq. (8). For example, the electronic state $A\,^2\Pi$ gives rise to two degenerate solutions labeled in MOLPRO as $|1.2\rangle = |\pi_x\rangle$ and $|1.3\rangle = |\pi_y\rangle$. The corresponding matrix representation of the $\hat{L}_z$ operator is not diagonal as computed by MOLPRO with the matrix elements being given, to within a global phase factor, by

$$\langle A\,^2\Pi, \pi_x|\hat{L}_z|A\,^2\Pi, \pi_x\rangle = 0, \tag{24}$$

$$\langle A\,^2\Pi, \pi_y|\hat{L}_z|A\,^2\Pi, \pi_y\rangle = 0, \tag{25}$$

$$\langle A\,^2\Pi, \pi_x|\hat{L}_z|A\,^2\Pi, \pi_y\rangle = -i. \tag{26}$$

Besides the matrix elements of $\hat{L}_x$ and $\hat{L}_y$ as well as the spin-orbit matrix elements are all complex numbers in the MOLPRO representation. The transformation from $|A\,^2\Pi, \pi_x$,

$S, \Sigma\rangle$ and $|A\,^2\Pi, \pi_y, S, \Sigma\rangle$ (MOLPRO) to our representation $|A\,^2\Pi, \Lambda = \pm 1, S, \Sigma\rangle$ (DUO) as defined by the conditions in Eqs. (8) and (9) is then given by

$$|\pm\Lambda\rangle = \frac{1}{\sqrt{2}}[\mp|x\rangle - i|y\rangle]. \quad (27)$$

In this representation, the matrix representations of all couplings relevant to this work are real, including that for $\hat{L}_z$ which is diagonal. For example, the $\hat{L}_x$ and $\hat{L}_y$ operators couple the X and A states via the following matrix elements in the MOLPRO representation:

$$\langle X\,^2\Sigma^+|\hat{L}_x|A\,^2\Pi, \pi_y\rangle = \langle X\,^2\Sigma^+|\hat{L}_y|A\,^2\Pi, \pi_x\rangle \equiv i l_{X-A}, \quad (28)$$

where l_{X-A} is a real number.

Applying Eq. (27) we obtain

$$L_{X-A} = -\sqrt{2}\, l_{X-A}. \quad (29)$$

Similarly, for the diagonal SO component coupling two components of the $A\,^2\Pi$ state, MOLPRO gives the following non-vanishing matrix elements:

$$\left\langle A\,^2\Pi, \pi_x, \Sigma = \tfrac{1}{2}\middle|\hat{H}_{\rm SO}\middle|A\,^2\Pi, \pi_y, \Sigma = \tfrac{1}{2}\right\rangle = i a_{A-A}, \quad (30)$$

$$\left\langle A\,^2\Pi, \pi_x, \Sigma = -\tfrac{1}{2}\middle|\hat{H}_{\rm SO}\middle|A\,^2\Pi, \pi_y, \Sigma = -\tfrac{1}{2}\right\rangle = -i a_{A-A}, \quad (31)$$

where a_{A-A} is a real number. These couplings in the representation of Eq. (27) become real

$$\mathrm{SO}_{A-A} = -a_{A-A}. \quad (32)$$

The (non-vanishing) non-diagonal SO-matrix elements in the MOLPRO representation

$$\begin{aligned}
&\left\langle X\,^2\Sigma^+, \Sigma = -\tfrac{1}{2}\middle|\hat{H}_{\rm SO}\middle|A\,^2\Pi, \pi_x, \Sigma = \tfrac{1}{2}\right\rangle = b_{X-A},\\
&\left\langle X\,^2\Sigma^+, \Sigma = -\tfrac{1}{2}\middle|\hat{H}_{\rm SO}\middle|A\,^2\Pi, \pi_y, \Sigma = \tfrac{1}{2}\right\rangle = i b_{X-A},\\
&\left\langle X\,^2\Sigma^+, \Sigma = \tfrac{1}{2}\middle|\hat{H}_{\rm SO}\middle|A\,^2\Pi, \pi_x, \Sigma = -\tfrac{1}{2}\right\rangle = -b_{X-A},\\
&\left\langle X\,^2\Sigma^+, \Sigma = \tfrac{1}{2}\middle|\hat{H}_{\rm SO}\middle|A\,^2\Pi, \pi_y, \Sigma = -\tfrac{1}{2}\right\rangle = i b_{X-A},\\
&\left\langle B\,^2\Sigma^+, \Sigma = -\tfrac{1}{2}\middle|\hat{H}_{\rm SO}\middle|A\,^2\Pi, \pi_x, \Sigma = \tfrac{1}{2}\right\rangle = b_{B-A},\\
&\left\langle B\,^2\Sigma^+, \Sigma = -\tfrac{1}{2}\middle|\hat{H}_{\rm SO}\middle|A\,^2\Pi, \pi_y, \Sigma = \tfrac{1}{2}\right\rangle = i b_{B-A},\\
&\left\langle B\,^2\Sigma^+, \Sigma = \tfrac{1}{2}\middle|\hat{H}_{\rm SO}\middle|A\,^2\Pi, \pi_x, \Sigma = -\tfrac{1}{2}\right\rangle = -b_{B-A},\\
&\left\langle B\,^2\Sigma^+, \Sigma = \tfrac{1}{2}\middle|\hat{H}_{\rm SO}\middle|A\,^2\Pi, \pi_y, \Sigma = -\tfrac{1}{2}\right\rangle = i b_{B-A},
\end{aligned}$$

b_{X-A} and b_{B-A} are real numbers. In our representations, the non-vanishing and symmetrically unique values are

$$\mathrm{SO}_{X-A} = \sqrt{2}\, b_{X-A}, \quad (33)$$

$$\mathrm{SO}_{B-A} = \sqrt{2}\, b_{B-A}. \quad (34)$$

The $\hat{L}^2$ term in Eq. (3) depends only on the internuclear distance and thus can be included into the functional forms of the potential energy functions or indirectly into the SO coupling terms, and thus can be excluded from our analysis. The vibrational basis functions $|\mathrm{state}, v\rangle$ are prepared as solutions of the pure vibrational uncoupled eigen-problems for a given adiabatic electronic "state"

$$\left[-\frac{\hbar^2}{2\mu}\frac{\partial^2}{\partial R^2} + V_{\rm state}(R)\right]|\mathrm{state}, v\rangle = E_v|\mathrm{state}, v\rangle, \quad (35)$$

using an equidistant grid representation.[47] Here, $V_{\rm state}$ is the corresponding potential energy function. For the $X\,^2\Sigma^+$, $A\,^2\Pi$, and $B\,^2\Sigma^+$ electronic states, we select 60, 50, and 40 lowest eigenfunctions, respectively, as contracted basis functions for the rovibronic problem. The vibrational matrix elements for all R-dependent terms appearing in the rovibronic Hamiltonian are evaluated numerically using the rectangle rule. We used an equidistant grid of 2001 points ranging from 1.1 to 2.7 Å.

Finally, the spin-rovibronic functions are symmetrized to be eigenfunctions of the parity operator $\sigma_v(xz)$ using Eq. (9). Thus, for each total angular momentum quantum number J up to 112.5 and each of two parities + and − a Hamiltonian matrix is generated and then diagonalized using the LAPACK routine DSYEVR as provided by the intel MKL libraries.

IV. REFINEMENT OF THE THEORETICAL RESULTS

Our *ab initio* calculations are some distance from achieving spectroscopic accuracy. In order to approach this level of accuracy, we refine the potential energy curves and coupling terms using experimental data and employing the program DUO. The best spectroscopic data are available in the form of measured transition frequencies with an uncertainty of 0.023 cm^{-1} by Saksena *et al.*[23] or 0.019 cm^{-1} by Launila and Berg[25] ($B - X$ and $A - X$ system). In order to improve the quality of the rovibronic energies, the underlying *ab initio* energies were refined by fitting to the experimental data from Launila and Berg,[25] as described below.

The least square fit both to energy levels (term values) and transition frequencies is implemented in DUO. We started by fitting energies, which is technically simpler than fitting frequencies. Vibrational states up to $v = 7$ in the case of $X\,^2\Sigma^+$, up to $v = 16$ in the case of $A\,^2\Pi$, and $v = 6$ for $B\,^2\Sigma^+$ were included. We used experimental line positions from Launila and Berg[25] and extracted the underlying energy levels using combination differences. A total of 5969 energy term values, with J up to 112.5, reproduce the 23 793 frequencies with the root-mean-square (rms) error of 0.07 cm^{-1}, with residuals varying up to 0.6 cm^{-1}. The latter value is several times larger than the rms errors stated by either Saksena *et al.*[23] or Launila and Berg,[25] which might indicate some assignment problems. Indeed, we found more than 2000 duplicate frequencies having the same values but very different assignments. Furthermore, the experimental set due to Launila and Berg[25] contains about 500 transitions that cannot be confirmed by combination differences. These transitions and the duplicates proved to be the largest outliers in our calculations.

The PECs were fitted using the Extended Morse Oscillator (EMOs) functions[44] given in the form

$$V(R) = T_{\rm e} + D_{\rm e}\left[1 - \exp\left(-\sum_{k=0}^{N} A_k \xi^k \left(R - R_{\rm e}\right)\right)\right]^2, \quad (36)$$

TABLE IV. Parameters for refined potential energy curves given using an extended Morse oscillatory form, see Eq. (36); units are cm^{-1} and Å.

Parameter	$X\,^2\Sigma^+$	$A\,^2\Pi^+$	$B\,^2\Sigma^+$
T_e	0.0	5405.85106434	20 688.31037841
$R_e = R_{ref}$	1.61890913	1.76905565	1.66807337
$T_e + D_e$	39 435.48544142	39 435.48544142	70 000.0
p_l	4	4	4
p_r	4	4	2
N_l	2	2	2
N_r	4	5	4
A_0	1.90354673020	1.52647207263	1.51006043336
A_1	− 0.10019383862	− 0.16794482851	− 0.14541739107
A_2	− 0.07118881034	0.05855136709	0.04527686438
A_3	− 0.23780463076	0.07637269923	1.28417838327
A_4	0.27801043427	− 0.14954775136	1.72071077730
A_5		0.32678665277	

where R_e is an equilibrium distance and ξ is the Šurkus-variable[48] given by

$$\xi = \left(\frac{R^p - R_{ref}^p}{R^p + R_{ref}^p}\right) \tag{37}$$

with p as a parameter. This form guarantees the correct dissociation limit and allows for extra flexibility in the degree of the polynomial on the left or on the right sides of a reference position R_{ref} which we take at $R_{ref} = r_e$. This is specified by the parameters $N = N_l$ (N_r) and $p = p_l$ (p_r), respectively (see Table IV which gives the final fitted PEC parameters). The functional form of Eq. (36) is adapted when implemented on the right side of $R_{ref} = r_e$ by changing N to N_r while, when used on the left side of $R_{ref} = r_e$ by changing N to N_l. Also the power of the radius entering the Šurkus variable changes into p_r, respectively, p_l according to the region that is modeled.

In the fits we used the same dissociation limit for the X and A states. The value that we determined is 39 435 cm^{-1} (4.89 eV) which can be compared to the published experimental values for the ground state dissociation energy D_e = 4.15 ± 0.05 eV[49] and 4.54 ± 0.01 eV.[50] The B state dissociation limit was constrained to lie 70 000 cm^{-1} above the ground state potential minimum which is close to value given by considering the excitation of atomic oxygen.

In order to describe the variation of the spin-orbit and electronic angular momentum couplings from the corresponding *ab initio* curves, we employed the morphing approach[51,52] as follows. A refined function $F(R)$ at a given grid point R_i ($i = 0 \ldots 2001$) is given by

$$F(R_i) = H(R_i) F^{ai}(R_i), \tag{38}$$

where $F^{ai}(R_i)$ is an *ab initio* function obtained from a sparse grid of 105 geometries using the cubic splines interpolation. The morphing function $H(R)$ is represented by a polynomial,[44]

$$H(R) = \left[(1-\xi)\sum_{k\geq 0}^{N_T} A_k \xi^k + \xi t_\infty\right], \tag{39}$$

in terms of the Šurkus variable ξ (Eq. (37)) with $p = 2$ and the reference geometry chosen as R_{ref} = 1.77 Å. Here, $t_\infty = 1$ is the value of the morphing function at $r \to \infty$ and the morphing expansion parameters are listed in Table V. For the interested reader, the supplementary material contains the final morphed curves on the fine grid.

TABLE V. Parameters of the refined morphing functions describing the SO and EAM functions of AlO (unitless), see Eqs. (38) and (39), as well of the empirical SR (cm^{-1}) and BOB corrections (unitless).

Object	A_0	A_1
SO_{A-A}	1.038991286985	− 0.039342225874
SO_{X-A}	0.882363315197	
SO_{B-A}	1.291104563209	
L_{X-A}	0.699772845944	
L_{B-A}	1.132563321574	
SR_X	0.006749015759	
SR_A	− 0.002060781906	
SR_B	− 0.001688949114	
BOB_X	0.001346178878	
BOB_A	0.001183536766	
BOB_B	0.001080261641	

In order to target the experimental accuracy, we had to add two types of empirical corrections not available in MOLPRO. To account for the Born-Oppenheimer-Breakdown (BOB) effect,[44] the rotational kinetic energy operator in Eq. (3) was replaced by

$$\frac{\hbar^2}{2\mu R^2} \to \frac{\hbar^2}{2\mu R^2}(1 + g^{BOB}(R)), \tag{40}$$

where the unitless BOB functions g^{BOB} are represented by the expansion in Eq. (39) with state-specific expansion parameters. The resulting empirical expansion parameters are given in Table V.

Finally, the spin-rotation (SR) couplings were also included as defined by

$$SR_X = \left\langle X\,^2\Sigma^+, \Lambda = 0, \Sigma = \tfrac{1}{2} \middle| \hat{H}_{SR} \middle| X\,^2\Sigma^+, \Lambda = 0, \Sigma = \tfrac{1}{2} \right\rangle, \tag{41}$$

$$SR_A = \left\langle A\,^2\Pi, \Lambda = 1, \Sigma = \tfrac{1}{2} \middle| \hat{H}_{SR} \middle| A\,^2\Pi, \Lambda = 1, \Sigma = \tfrac{1}{2} \right\rangle, \tag{42}$$

$$SR_B = \left\langle B\,^2\Sigma^+, \Lambda = 0, \Sigma = \tfrac{1}{2} \middle| \hat{H}_{SR} \middle| B\,^2\Sigma^+, \Lambda = 0, \Sigma = \tfrac{1}{2} \right\rangle, \tag{43}$$

where the effective spin-rotational Hamiltonian term H_{SR} is given by[46]

$$\hat{H}_{SR} = \gamma(R)(\hat{J} - \hat{L} - \hat{S}) \cdot \hat{S}. \tag{44}$$

We also used Eq. (39) to represent the SR couplings $\gamma(R)$ analytically. The expansion parameters obtained through the fits to the experimental data are listed in Table V.

In the refinement up to 28 experimental energy levels per value of the quantum number J for even and odd parity states were used. The goal of this process is to obtain the best fit with the minimal number of parameters to ensure that the resulting model is capable of giving high accuracy predictions

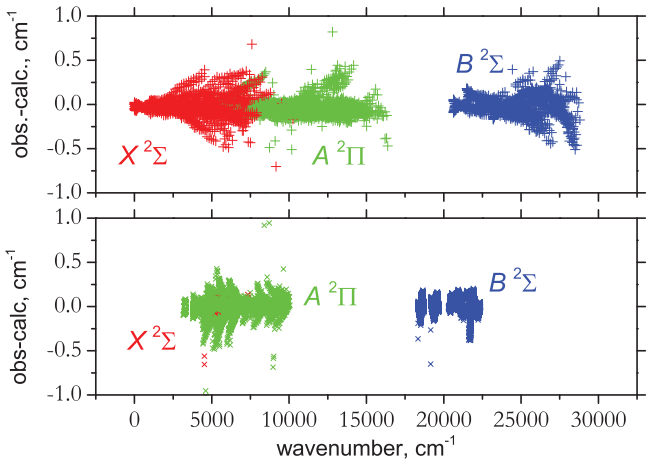

FIG. 4. Residuals (observed-calculated, cm^{-1}) for energies (upper display) and frequencies (lower display) of $^{27}Al^{16}O$: The calculated values are obtained from our refined PECs, SOs, and EAMCs, while the observed are by Launila and Berg.[25]

that extend beyond the range of experimental data. The first step was to obtain the most accurate fit for low-lying energies which involved mainly the refinement of the lowest electronic state. In the fitting the shapes of refined curves are controlled and (partially) constrained to the corresponding original *ab initio* curves along the idea used successfully for polyatomic molecules.[53–55] The program DUO allows the use of factors giving the relative weights to the *ab initio* or experimental data in a given fit. The fitting procedure started with a strong *ab initio* bias, but slowly increased the weight of the experimental fit up to a match with the weight for the *ab initio* fit. At this point, the overall shape of the curves was preserved but the accuracy was still not ideal. In order to improve on this, we continued to increase the weight for the experimental results. In this way, we obtained the equilibrium positions compatible with experiment, implicitly allowing flexibility in performing the refinement. When the lower energy term values were reproduced with a rms deviation better than 0.08 cm^{-1} we added the higher electronic states, namely, the $A\,^2\Pi$ and $B\,^2\Sigma^+$ states. Optimization for the $B\,^2\Sigma^+$ state was straightforward. For the $A\,^2\Pi$ state, extra care was needed due to the fact that the spin-orbit coupling manifests itself by splitting the potential energy curve. This made the accurate fitting to experiment more difficult.

Considering all the corrections and the refinement techniques used the energy levels obtained are in reasonable agreement with the observed ones up to the desired value of $J = 112.5$ and our final fit reproduces our entire data set of energies with a rms error of 0.08 cm^{-1}. At this stage, the experimental frequencies were added to the fit in order to exclude possible artefacts associated with the energy fit. The final rms error of the combined fit to both energies and frequencies is 0.07 cm^{-1}, which is consistent with the error of our combination difference procedure (see above). The rms error of the frequencies only is 0.06 cm^{-1}. A more detailed, graphical representation of the quality of the fit is shown in Fig 4, where Obs.−Calc. residuals for the energies and frequencies are presented.

The fitting algorithms described above have been implemented as a standard part of DUO. Convergence of the refinement algorithm is fast, accurate fits being obtained in less than 10 iterations. The resulting numerical refined curves are in good agreement with the *ab initio* calculations for the range we are interested in, see Fig. 1.

Figure 3 also compares our *ab initio* and refined angular momentum coupling matrix element curves. These couplings are actually rather small and not too much significance should be given to the differences between the *ab initio* and refined values. The refinement of the coupling curves however deserves some attention: first, one can see from Fig. 3 that the

TABLE VI. Comparison of "observed"[23] and calculated $J = 0.5$ rovibronic energy levels for $^{27}Al^{16}O$ in cm^{-1}. The electronic states are labelled X, A, and B for $X\,^2\Sigma^+$, $A\,^2\Pi$, and $B\,^2\Sigma^+$, respectively. $p = \pm$ is the total parity and $\Omega = \Lambda + \Sigma$.

J	p	State	v	$\lvert\Omega\rvert$	Obs.	Calc.	Obs.−Calc.	J	p	State	v	$\lvert\Omega\rvert$	Obs.	Calc.	Obs.−Calc.
0.5	+	X	0	0.5	0.0000	0.0000	0.0000	0.5	…	X	0	0.5	1.2259	1.2742	−0.0483
0.5	+	X	1	0.5	965.4519	965.4355	0.0164	0.5	…	X	1	0.5	966.6633	966.6994	−0.0361
0.5	+	X	2	0.5	1916.8596	1916.8454	0.0142	0.5	…	X	2	0.5	1918.0589	1918.0993	−0.0404
0.5	+	X	3	0.5	2854.2366	2854.2063	0.0303	0.5	…	X	3	0.5	2855.4091	2855.4508	−0.0417
0.5	+	X	4	0.5	3777.5016	3777.5042	−0.0026	0.5	…	X	4	0.5	3778.6781	3778.7404	−0.0623
0.5	+	X	5	0.5	4686.7136	4686.6609	0.0527	0.5	…	X	5	0.5	4687.8785	4687.8919	−0.0134
0.5	+	A	0	0.5	5346.1146	5346.1164	−0.0018	0.5	…	X	6	0.5	5583.0853	5583.1308	−0.0455
0.5	+	X	6	0.5	5581.9326	5581.9076	0.0250	0.5	…	X	7	0.5	6464.2647	6464.2586	0.0061
0.5	+	A	1	0.5	6067.0507	6066.9348	0.1159	0.5	…	B	0	0.5	20 636.4057	20 636.4968	−0.0911
0.5	+	X	7	0.5	6463.1256	6463.0405	0.0851	0.5	…	B	1	0.5	21 499.5010	21 499.4728	0.0282
0.5	+	B	0	0.5	20 635.3658	20 635.3089	0.0569	0.5	…	B	2	0.5	22 355.2627	22 355.3500	−0.0873
0.5	+	B	1	0.5	21 498.4723	21 498.2939	0.1784	0.5	…	B	3	0.5	23 203.6592	23 203.8278	−0.1686
0.5	+	B	2	0.5	22 354.2179	22 354.1801	0.0378	0.5	…	B	4	0.5	24 044.7784	24 044.9011	−0.1227
0.5	+	B	3	0.5	23 202.6463	23 202.6668	−0.0205	0.5	…	B	5	0.5	24 878.5385	24 878.5962	−0.0577
0.5	+	B	4	0.5	24 043.7747	24 043.7490	0.0257	0.5	…	B	6	0.5	25 705.0220	25 704.9628	0.0592
0.5	+	B	5	0.5	24 877.5507	24 877.4529	0.0978	0.5	…	B	7	0.5	26 524.1323	26 524.0736	0.0587
0.5	+	B	6	0.5	25 704.0201	25 703.8281	0.1920	0.5	…	B	8	0.5	27 335.9454	27 336.0012	−0.0558
0.5	+	B	7	0.5	26 523.1582	26 522.9476	0.2106								
0.5	+	B	8	0.5	27 334.9814	27 334.8839	0.0975								

TABLE VII. Comparison of "observed"[23] and calculated $J = 20.5$ rovibronic energy levels for $^{27}Al^{16}O$ in cm^{-1}. The electronic states are labelled X, A, and B for $X\,^2\Sigma^+$, $A\,^2\Pi$, and $B\,^2\Sigma^+$, respectively. $p = \pm$ is the total parity and $\Omega = \Lambda + \Sigma$.

J	p	State	v	$\lvert\Omega\rvert$	Obs.	Calc.	Obs.−Calc.	J	p	State	v	$\lvert\Omega\rvert$	Obs.	Calc.	Obs.−Calc.
20.5	+	X	0	0.5	267.9631	267.9590	0.0041	20.5	...	X	0	0.5	294.6449	294.6783	−0.0334
20.5	+	X	1	0.5	1230.9683	1230.9426	0.0257	20.5	...	X	1	0.5	1257.4645	1257.4451	0.0194
20.5	+	X	2	0.5	2179.9341	2179.8837	0.0504	20.5	...	X	2	0.5	2206.1383	2206.1765	−0.0382
20.5	+	X	3	0.5	3114.8483	3114.7564	0.0919	20.5	...	X	3	0.5	3140.7580	3140.8524	−0.0944
20.5	+	X	4	0.5	4035.5059	4035.5384	−0.0325	20.5	...	X	4	0.5	4061.4727	4061.4633	0.0094
20.5	+	X	5	0.5	4942.1716	4942.1161	0.0555	20.5	...	X	5	0.5	4968.0439	4967.9399	0.1040
20.5	+	A	0	1.5	5451.4162	5451.3967	0.0195	20.5	...	A	0	1.5	5451.3854	5451.3959	−0.0105
20.5	+	A	0	0.5	5582.1073	5582.1146	−0.0073	20.5	...	A	0	0.5	5581.9590	5581.9570	0.0020
20.5	+	X	6	0.5	5834.7763	5834.7255	0.0508	20.5	...	X	6	0.5	5860.5021	5860.4165	0.0856
20.5	+	A	1	1.5	6169.7622	6169.7762	−0.0140	20.5	...	A	1	1.5	6169.7682	6169.7739	−0.0057
20.5	+	A	1	0.5	6300.8068	6300.8057	0.0011	20.5	...	A	1	0.5	6300.5456	6300.5415	0.0041
20.5	+	X	7	0.5	6713.0810	6713.0702	0.0108	20.5	...	X	7	0.5	6738.7119	6738.6790	0.0329
20.5	+	A	2	1.5	6879.2183	6879.2299	−0.0116	20.5	...	A	2	1.5	6879.2277	6879.2338	−0.0061
20.5	+	A	2	0.5	7010.8582	7010.8581	0.0001	20.5	...	A	2	0.5	7010.4510	7010.4400	0.0110
20.5	+	A	3	1.5	7583.0560	7583.0544	0.0016	20.5	...	A	3	1.5	7578.7530	7578.7527	0.0003
20.5	+	A	3	0.5	7713.5451	7713.5466	−0.0015	20.5	...	A	3	0.5	7713.0098	7712.9986	0.0112
20.5	+	A	4	1.5	8271.2237	8271.2351	−0.0114	20.5	...	A	4	1.5	8271.2667	8271.2750	−0.0083
20.5	+	A	4	0.5	8389.4431	8389.3856	0.0575	20.5	...	A	4	0.5	8395.4943	8395.4619	0.0324
20.5	+	A	5	1.5	8954.4210	8954.4448	−0.0238	20.5	...	A	5	1.5	8954.4477	8954.4595	−0.0118
20.5	+	A	5	0.5	9081.9571	9081.9387	0.0184	20.5	...	A	5	0.5	9082.8551	9082.8333	0.0218
20.5	+	A	6	1.5	9629.0535	9629.0716	−0.0181	20.5	...	A	6	1.5	9629.0791	9629.0794	−0.0003
20.5	+	A	6	0.5	9757.8668	9757.8426	0.0242	20.5	...	A	6	0.5	9758.2129	9758.1954	0.0175
20.5	+	A	7	1.5	10 295.2860	10 295.2687	0.0173	20.5	...	A	7	1.5	10 295.2540	10 295.2744	−0.0204
20.5	+	A	7	0.5	10 424.7133	10 424.6719	0.0414	20.5	...	A	7	0.5	10 424.8274	10 424.7969	0.0305
20.5	+	A	8	1.5	10 953.3057	10 953.2833	0.0224	20.5	...	A	8	1.5	10 953.4767	10 953.4488	0.0279
20.5	+	A	8	0.5	11 083.5113	11 083.3520	0.1593	20.5	...	B	0	0.5	20 912.8996	20 912.9072	−0.0076
20.5	+	B	0	0.5	20 888.0099	20 888.0017	0.0082	20.5	...	B	1	0.5	21 773.9569	21 773.8063	0.1506
20.5	+	B	1	0.5	21 749.2138	21 749.0901	0.1237	20.5	...	B	2	0.5	22 627.6489	22 627.6188	0.0301
20.5	+	B	2	0.5	22 603.0883	22 603.0910	−0.0027	20.5	...	B	3	0.5	23 473.9668	23 474.0508	−0.0840
20.5	+	B	3	0.5	23 449.6901	23 449.7099	−0.0198	20.5	...	B	4	0.5	24 313.0009	24 313.0930	−0.0921
20.5	+	B	4	0.5	24 288.9280	24 288.9381	−0.0101	20.5	...	B	5	0.5	25 144.7235	25 144.7776	−0.0541
20.5	+	B	5	0.5	25 120.9127	25 120.8067	0.1060	20.5	...	B	6	0.5	25 969.2918	25 969.1497	0.1421
20.5	+	B	6	0.5	25 945.4391	25 945.3620	0.0771	20.5	...	B	7	0.5	26 786.3831	26 786.2835	0.0996
20.5	+	B	7	0.5	26 762.8339	26 762.6773	0.1566	20.5	...	B	8	0.5	27 596.1797	27 596.2549	−0.0752
20.5	+	B	8	0.5	27 572.8201	27 572.8286	−0.0085								

spin-orbit coupling responsible for the splitting of the $A\,^2\Pi$ state is modified very little by the fitting to the experimental values. The same is true for the spin-orbit coupling between the state $A\,^2\Pi$ and $X\,^2\Sigma^+$. We note that (i) the $B\,^2\Sigma^+$ curve actually undergoes many crossings with electronic states which are high-lying near equilibrium, see Liu *et al.*,[30] for example, and which we do not consider and (ii) in the absence of the crossings with the $A\,^2\Pi$, its effect on the energies is small. It is likely that the refinement of this coupling curve would need to be attempted to recover other non-adiabatic effects not included in our *ab initio* treatment. Also, our calculation does not include hyperfine splitting. This is found to be comparable to the accuracy of our fit and can be considered a relevant explanation for our residual uncertainties. All the *ab initio* and refined curves used in the DUO calculations are given in the supplementary material.[56]

Tables VI and VII give samples of the energy values obtained after the refinement compared to the experimentally derived values. Our new results are in reasonable agreement with the experiment. It should also be noted that the "Obs" columns list term values derived from the experiment using the combinational differences (see above). The complete table where our term values are compared to the experimentally derived term values is given in the supplementary material,[56] which also contains a similar comparison for the wavenumbers from Launila and Berg.[25]

V. CONCLUSION

The goal of this work was to obtain a reliable *ab initio* representation of the first three potential energy states of aluminum monoxide, and to use these to provide an accurate fit for the potential energy curves and various coupling terms to available experimental data. The rovibronic energy levels are calculated using a new code[45] for computing spectra for arbitrarily coupled diatomic potentials. The resulting levels and associated transition frequencies are suitable for the construction of a comprehensive line list for AlO. This will be the subject of future work.[57]

ACKNOWLEDGMENTS

This work is supported by ERC Advanced Investigator Project No. 267219. We thank L. Lodi and A. Stolyarov for their helpful discussions and suggestions.

[1]E. D. Tenenbaum and L. M. Ziurys, Astrophys. J. **694**, L59 (2009).
[2]A. Bernard and R. Gravina, Z. Naturforsch. A **39**, 1049 (1984).
[3]D. P. K. Banerjee, R. J. Barber, N. K. Ashok, and J. Tennyson, Astrophys. J. **627**, L141 (2005).
[4]D. P. K. Banerjee, W. P. Varricatt, B. Mathew, O. Launila, and N. M. Ashok, Astrophys. J. Lett. **753**, L20 (2012).
[5]P. Sriramachandran, B. Viswanathan, and R. Shanmugavel, Sol. Phys. **286**, 315 (2013).
[6]E. R. Johnson, J. Geophys. Res. **70**, 1275, doi:10.1029/JZ070i005p01275 (1965).
[7]N. W. Rosenberg, D. Golomb, and E. F. Allen, J. Geophys. Res. **69**, 1451, doi:10.1029/JZ069i007p01451 (1964).
[8]J. L. Gole and C. E. Kolb, J. Geophys. Res., [Space Phys.] **86**, 9125, doi:10.1029/JA086iA11p09125 (1981).
[9]D. J. Knecht, C. P. Pike, E. Murad, and D. L. A. Rall, J. Spacecrafts Rockets **33**, 677 (1996).
[10]B. Bescos, G. Morley, and A. G. Urena, Chem. Phys. Lett. **244**, 407 (1995).
[11]C. Naulin and M. Costes, Chem. Phys. Lett. **310**, 231 (1999).
[12]N. G. Glumac, J. Servaites, and H. Krier, Combust. Sci. Technol. **172**, 97 (2001).
[13]S. D. Zhang and H. Y. Li, Chem. Res. Chin. Univ. **19**, 320 (2003).
[14]W. C. Pomeroy, Phys. Rev. **29**, 59 (1927).
[15]M. K. Sen, Ind. J. Phys. **11**, 251 (1937).
[16]A. Lagerqvist, N. E. L. Nilsson, and R. F. Barrow, Ark. Fys. **12**, 543 (1957).
[17]J. M. Mahieu, D. Jacquniot, J. Schamps, and J. A. Hall, J. Phys. B **8**, 308 (1975).
[18]S. Rosenwaks, R. E. Steele, and H. P. Broida, J. Chem. Phys. **63**, 1963 (1975).
[19]J. Schamps, Chem. Phys. **2**, 352 (1973).
[20]M. Singh and M. D. Saksena, Can. J. Phys. **59**, 955 (1981).
[21]J. Jin, Y. Chen, L. S. Pei, C. J. Hu, X. X. Ma, and C. X. Chen, Acta Phys. Sin. **49**, 1689 (2000).
[22]D. Kraus, R. J. Saykally, and V. E. Bondybey, ChemPhysChem **3**, 364 (2002).
[23]M. D. Saksena, M. N. Deo, K. Sunanda, S. H. Behere, and C. T. Londhe, J. Mol. Spectrosc. **247**, 47 (2008).
[24]K. P. Huber and G. Herzberg, *Molecular Spectra and Molecular Structure IV. Constants of Diatomic Molecules* (Van Nostrand Reinhold Company, New York, 1979).
[25]O. Launila and L.-E. Berg, J. Mol. Spectrosc. **265**, 10 (2011).
[26]G. Orlova and J. D. Goddard, Mol. Phys. **98**, 961 (2000).
[27]H. Partridge, S. R. Langhoff, B. H. Lengsfield, and B. Liu, J. Quant. Spectrosc. Radiat. Transfer **30**, 449 (1983).
[28]N. Honjou, J. Mol. Struct.: THEOCHEM **939**, 59 (2010).
[29]N. Honjou, Comput. Theor. Chem. **978**, 138 (2011).
[30]H. Liu, D. Shi, J. Sun, and Z. Zhu, Spectra Chim. Acta A **101**, 400 (2013).
[31]B. H. Lengsfield and B. Liu, J. Chem. Phys. **77**, 6083 (1982).
[32]C. Zenouda, P. Blottiau, G. Chambaud, and P. Rosmus, J. Mol. Struct.: THEOCHEM **458**, 61 (1998).
[33]J. Tennyson and S. N. Yurchenko, Mon. Not. R. Astron. Soc. **425**, 21 (2012).
[34]B. Yadin, T. Vaness, P. Conti, C. Hill, S. N. Yurchenko, and J. Tennyson, Mon. Not. R. Astron. Soc. **425**, 34 (2012).
[35]E. J. Barton, S. N. Yurchenko, and J. Tennyson, Mon. Not. R. Astron. Soc. **434**, 1469–1475 (2013).
[36]E. J. Barton, C. Chiu, S. Golpayegani, S. N. Yurchenko, J. Tennyson, D. J. Frohman, and P. F. Bernath, Mon. Not. R. Astron. Soc. **442**, 1821 (2014).
[37]H. J. Werner, P. J. Knowles, R. Lindh, F. R. Manby, and M. Schütz, MOLPRO, version 2010.1, a package of *ab initio* programs 2010, see http://www.molpro.net/.
[38]H.-J. Werner, P. J. Knowles, G. Knizia, F. R. Manby, and M. Schütz, WIREs Comput. Mol. Sci. **2**, 242 (2012).
[39]O. Launila and J. Jonsson, J. Mol. Spectrosc. **168**, 1 (1994).
[40]M. D. Saksena, G. S. Ghodgaonkar, and M. Singh, J. Phys. B **22**, 1993 (1989).
[41]J. Tennyson, J. Mol. Spectrosc. **298**, 1 (2014).
[42]H. Ito and M. Goto, Chem. Phys. Lett. **227**, 293 (1994).
[43]Y. Ralchenko, A. E. Kramida, J. Reader, and NIST ASD Team, *NIST Atomic Spectra Database (version 3.1.5)* (NIST, 2008), see http://www.nist.gov/pml/data/asd.cfm.
[44]R. J. Le Roy, "LEVEL 8.0: A computer program for solving the radial Schrödinger equation for bound and quasibound levels," University of Waterloo Chemical Physics Research Report CP-663, 2007, see http://leroy.uwaterloo.ca/programs/.
[45]S. N. Yurchenko and *et al.*, "Duo: A program for solving the coupled radial Schrödinger equation for open shell-diatomic molecules" (unpublished).
[46]H. Kato, Bull. Chem. Soc. Jpn. **66**, 3203 (1993).
[47]J. W. Cooley, Math. Comput. **15**, 363 (1961); available at http://www.ams.org/journals/mcom/1961-15-076/S0025-5718-1961-0129566-X/home.html.
[48]A. A. Šurkus, R. J. Rakauskas, and A. B. Bolotin, Chem. Phys. Lett. **105**, 291 (1984).
[49]N. S. Murthy, S. P. Bagare, and B. N. Murthy, J. Quant. Spectrosc. Radiat. Transfer **19**, 455 (1978).
[50]D. C. Tyte, Proc. Phys. Soc. London **92**, 1134 (1967).
[51]M. Meuwly and J. M. Hutson, J. Chem. Phys. **110**, 8338 (1999).
[52]S. Skokov, K. A. Peterson, and J. M. Bowman, Chem. Phys. Lett. **312**, 494 (1999).
[53]S. N. Yurchenko, B. A. Voronin, R. N. Tolchenov, N. Doss, O. V. Naumenko, W. Thiel, and J. Tennyson, J. Chem. Phys. **128**, 044312 (2008).
[54]A. Yachmenev, S. N. Yurchenko, P. Jensen, and W. Thiel, J. Chem. Phys. **134**, 244307 (2011).
[55]S. N. Yurchenko and J. Tennyson, Mon. Not. R. Astron. Soc. **440**, 1649 (2014).
[56]See supplementary material at http://dx.doi.org/10.1063/1.4897484 for (a) an excel spreadsheet containing the *ab initio* and refined potential energy curves and couplings; (b) a readme file explaining the contents of the spread sheet.
[57]S. N. Yurchenko, L. Lodi, and J. Tennyson, "ExoMol molecular line lists: VIII The spectrum of AlO," Mon. Not. R. Astron. Soc. (to be published).